

修士論文：

多成分プラズマにおける重イオンの波動による新しい加熱過程

水田孝信

指導教官 星野真弘 教授

東京大学大学院理学系研究科地球惑星科学専攻

(2002年2月28日)

概要

テスト粒子シミュレーションを用いて、有限振幅の電磁流体 (MHD) 波動中の、陽子より重い荷電粒子 (重イオン) の選択的強い加熱を研究した。電子、陽子、重イオンで構成される 3 成分プラズマ中では、波動モードの一つは、長波長において、Alfvén 速度より非常に速い位相速度を持つ。この波動と、他の Alfvén 波動と共鳴することにより、重イオンは背景磁場に対して、垂直方向に強く非等方加熱される。我々は、3 成分プラズマ中での、重イオンの新たな加熱モデルを提案し、その新しいモデルがテスト粒子シミュレーションと良くあう事を示す。新しいモデルを検証するため、2 つの波の振幅依存性について調べた。この新しい加熱過程は、電子と陽子のみで構成される 2 成分プラズマの単純な延長では説明出来ないと考えられる。

謝辞

本研究は星野真弘教授の指導の下で行いました。教授の多大なご指導にこそより感謝いたします。また、この論文を丁寧に査読され、有用で的確な助言を頂き、感謝いたします。

寺澤敏夫教授には有用な議論、助言を頂き感謝いたします。また、東京大学S T P (太陽地球間物理)グループのスタッフ、学生の方々に感謝いたします。

また、岩垂奨学会には多大なご支援を頂き、感謝いたします。奨学会の発展に大きく貢献された故岩垂孝一氏に深く感謝するとともに、ご冥福をお祈りいたします。

Master Thesis:

New wave heating process of heavy ions in multi-component plasmas

Takanobu Mizuta

Supervisor: Prof. Masahiro Hoshino

Department of Earth and Planetary Science, Graduate School of Science, University of Tokyo

(February 25, 2002)

Abstract

We discuss preferential, strong heating of heavier charged particles than protons in large amplitude magnetohydrodynamic (MHD) waves by using test particle simulations. In a 3 component plasma that consists of electrons, protons and heavy ions, one of the wave branches has phase velocity larger than the Alfvén velocity in a long wavelength regime. We find that the resonant interaction between this wave and the other Alfvén wave leads the heavy ions to strong anisotropic heating in perpendicular direction to an ambient magnetic field. We propose a new heating model for the heavy ions in the 3 component plasma, and the new model takes a good agreement with the test particle simulations. To confirm the new model, we also study the dependence of the amplitudes of these two waves. We consider that this new heating process is not explained by a simple extension of the plasma heating process understood in a 2 component plasma which consists of electrons and protons.

ACKNOWLEDGMENTS

The present thesis has been achieved being supervised by Professor M. Hoshino, the author would like to express sincere and hearty appreciation to him for his guidance and great help to this work and for his careful reading of the manuscript and useful suggestion for revision.

The author would like to thank Professor T. Terasawa for valuable discussion and comments. The author is also very much grateful to staffs and graduate students of STP (solar terrestrial physics) group at the University of Tokyo.

Contents

概要	i
謝辞	ii
Abstract	iii
Acknowledgments	iv
Contents	v
I INTORODUCTION	1
II PARTICLE MOTION IN ONE EMIC WAVE	4
A Dispersion relation for the multi-component plasma	4
B Pitch-angle scattering in a EMIC wave	5
III NUMERICAL STUDY	8
A Simulation model	8
B Result for protons	9
C Result for heavy ions	10
IV THEORY	12
A Explanation by ε and χ	12
B Purely electric and magnetic waves theory	13
V DEPENDENCE OF WAVE AMPLITUDES	17
A Dependence of wave amplitudes for heavy ions	17
B Case of weak SPA	18
C Case of strong SPA	19
D Dependence of wave amplitudes for protons	20
E Dependence of wave amplitudes in the 2 component plasma	20
VI SUMMARY AND DISSCUSION	22

References	24
Tables	26
Figures	27

I. INTRODUCTION

Preferential heating of heavier charged particles than protons is observed in several plasma circumstances. The observations of the Ultraviolet Coronagraph Spectrometer (UVCS) operating onboard the *Solar and Heliospheric Observatory (SOHO)* satellite indicate that in the polar coronal holes the temperature ratio between O^{5+} and protons is much larger than their mass ratio¹, $T_{O^{5+}}/T_p > m_{O^{5+}}/m_p$, where T is the temperature, m is the mass, respectively. (The subscripts “ O^{5+} ” and “ p ” stand for the O^{5+} and the protons, respectively.) The observations also indicate that O^{5+} has a highly anisotropic temperature: the temperature in the perpendicular direction to the magnetic field is 10 - 100 times hotter than that in the parallel direction to the magnetic field. This observation implies the existence of preferential heating processes of heavy ions to the perpendicular direction for the magnetic field. Fast Auroral Snapshot (FAST) and Freja satellites observed preferential heating of He^+ ions to the perpendicular direction for the terrestrial magnetic field in the terrestrial auroral region^{2,3}. This heating occurs in association with electromagnetic ion cyclotron (EMIC) waves, which implies that the He^+ are heated through a cyclotron resonance with the waves. For these studies, it is very important to understand the wave-particle interaction for the heavy ions.

Many authors have examined preferential heating of heavy ions. Tanaka⁴ has performed numerical simulations and indicated that the heavy ions are preferentially heated in EMIC waves driven by thermal anisotropic instability of protons. He discovered that the velocities of most heavy ions direct to the electric field of the excited waves, and the heavy ions are strongly heated to the perpendicular direction for an ambient magnetic field by experiencing the electric field of the waves. The quasi linear theory⁵, assuming that the phase between particles and waves is random, cannot explain this heating because this heating occurs by persisting a specific phase relation between the heavy ions velocity and waves. In fact, in the framework of the quasi linear theory under a weak turbulence, it has been analytically showed that the heating process of the heavy ions does not have a qualitative difference from

the heating process of the protons⁶. These facts indicate that the phase between particles and waves is quite important information for the strong heating.

Isenberg⁷ has pointed out that heavy ions can be effectively heated by the second order Fermi acceleration, because they can interact with EMIC mode in two resonant points while protons can interact with the EMIC mode in only one resonant point in the solar wind. Mizuta and Hoshino⁸ have indicated that there is a very fast EMIC mode in a 3 component plasma that consists of electrons, protons, and heavy ions, which mode does not exist in the 2 component plasma that consists of electrons and protons, and this mode plays an important role for the preferential heating of the heavy ions. Theoretical studies such as beam instability, parametric instability and so on in the multi component plasma indicate that several wave modes can be excited, which modes are never excited in the 2 component plasma⁹⁻¹¹. These facts indicate that, what the heavy ions resonate with the waves which cannot resonate with the protons causes the preferentiality of the heavy ions.

Theses studies implied that properties of wave-particle interaction in the multi component plasma are qualitatively different from that in the 2 component plasma, and simply extension of the theory on the 2 component plasma will not explain the phenomena in the multi component plasma. For understanding the preferential heating, it is important to examine the wave-particle interaction of the heavy ions in the multi-component plasma taking account of the phase relation between the heavy ions and the waves.

In this thesis, we discuss by using test particle simulations that heavy ions are preferentially and strongly heated by the resonant interaction between a high-frequency EMIC wave and a low-frequency MHD wave if the two waves have almost same Poynting fluxes in the 3 component plasma. We propose a new wave heating model explaining the preferential and strong heating of heavy ions, and show that the model is good agreement with the test particle simulations.

The plan of this thesis is as follows. In Section II, we briefly review the dispersion relation in the multi component plasma and the pitch-angle scattering in one coherent EMIC wave. In Section III, we develop test particle simulations and show details of result in the

case of protons and heavy ions, respectively. In Section IV, we propose a new model for preferential and strong heating of heavy ions in the multi component plasma. In Section V, we examine the dependence of the wave amplitudes, and we show that the new model take good agreement with the test particle simulations.

II. PARTICLE MOTION IN ONE EMIC WAVE

A. Dispersion relation for the multi-component plasma

We only treat circularly polarized waves propagating along the ambient magnetic field (B_0) in a cold plasma. We assume that the wave frequency (ω) is much smaller than the electron cyclotron frequency (Ω_e). The dispersion relation in the 2 component plasma that consists of electrons and protons is

$$\frac{\omega^2}{k^2} = V_A^2 \left(1 - \frac{\omega}{\Omega_p} \right), \quad (1)$$

where k is the wave number, V_A is the Alfvén velocity and Ω_p is the proton cyclotron frequency. We define the sign of ω and the phase velocity $V_{\text{ph}} \equiv \omega/k$ as follows: when a wave is left-hand circularly polarized (right-hand circularly polarized), we take $\omega > 0$ ($\omega < 0$), when the wave having phase velocity parallel (antiparallel) to the ambient field, we take $V_{\text{ph}} > 0$ ($V_{\text{ph}} < 0$). The top of Figure 1 shows this dispersion relation. The brunch having $\omega < 0$ is a whistler mode, and that having $\omega > 0$ is an EMIC mode. When $k \ll \Omega_p/V_A$ (the reciprocal of the proton inertial length), these two modes degenerate to the non-dispersive shear Alfvén wave which dispersion relation is given as $\omega/k = V_A$. As $k \rightarrow \infty$, the frequency of the EMIC mode asymptotically approaches Ω_p , while the whistler mode extends to the wave brunch having the larger velocity than the Alfvén velocity.

The dispersion relation in the 3 component plasma that consists of electrons, protons and heavy ions is

$$\frac{(1-f)\Omega_p}{\Omega_p - \omega} + \frac{\Omega_h f}{\Omega_h - \omega} - \frac{k^2 V_A^2}{\omega \Omega_p} = 1, \quad (2)$$

where $f \equiv q_h n_h / (|q_e| n_e)$ (q is the charge of the particle, m is the mass, n is the number density) and the subscript denotes “e”, “p” and “h” denote electrons, protons and heavy ions, respectively. The bottom of Figure 1 shows this dispersion relation. The EMIC mode separates two brunches, Lp mode (the brunch approaching $\omega \rightarrow \Omega_p$) and Lh mode (the brunch approaching $\omega \rightarrow \Omega_h$). When $k \ll \Omega_p/V_A$, Lh mode is nondispersive shear Alfvén

wave like 2 component plasma. On the other hand, Lp mode has finite frequency (ω_{co}) when $k \rightarrow 0$. This cut-off frequency ω_{co} is,

$$\omega_{co} = f\Omega_p + (1 - f)\Omega_h. \quad (3)$$

Lp mode has very faster phase velocity than Alfvén velocity and has very long wavelength near the cut-off frequency. We call the Lp mode near the cut-off frequency “Super Alfvénic EMIC wave” (SPA) and call the Lp mode having not so faster phase velocity than Alfvén velocity and Lh mode “Sub Alfvénic EMIC wave” (SBA). Lh mode is categorized into the SBA regardless of wave number k . Roughly speaking, Lp mode at $k \gtrsim \Omega_p/V_A$ is categorized into the SBA and Lp mode at $k \rightarrow 0$ is categorized into the SPA. It is very important that the SPA never exists in the 2 component plasma. Following sections, we show that there is a qualitative big difference between the properties of wave-particle interaction in the 2 component plasma and that in the 3 component plasma.

B. Pitch-angle scattering in a EMIC wave

The behavior of a test particle in a monochromatic wave is well studied so far^{12,13}. The test particles obey the following equations of motion,

$$\frac{dv_{\parallel}}{dt} = \eta\Omega v_{\perp} \sin \psi, \quad (4)$$

$$\frac{dv_{\perp}}{dt} = -\eta\Omega(v_{\parallel} - \frac{\omega}{k}) \sin \psi, \quad (5)$$

$$\frac{d\psi}{dt} = -k(v_{\parallel} - V_R) + \frac{\eta\Omega}{v_{\perp}}(\frac{\omega}{k} - v_{\parallel}) \cos \psi, \quad (6)$$

where v_{\parallel} and v_{\perp} are the test particle velocity components parallel and perpendicular to the ambient magnetic field, respectively. Ω is the gyro frequency for the test particle, ψ is the difference between the phase angle of v_{\perp} and that of the wave magnetic field (B_{\perp}), and $\eta \equiv B_{\perp}/B_0$. V_R is the resonant velocity defined as

$$V_R = \frac{\omega - \Omega}{k}. \quad (7)$$

From these equations, we obtain the two constants of motion,

$$(v_{\parallel} - \frac{\omega}{k})^2 + v_{\perp}^2 \equiv \varepsilon, \quad (8)$$

$$\frac{1}{2}(v_{\parallel} - V_R)^2 - \eta v_{\perp} \frac{\Omega}{k} \cos \psi \equiv \chi. \quad (9)$$

Eq. (8) means the energy conservation in the wave frame and shows that the particle motions are constrained to a constant ε circle in $(v_{\parallel}, v_{\perp})$ space (Figure 2 a). Eq. (9) shows that the test particles satisfying the cyclotron resonant condition ($v_{\parallel} \simeq V_R$) are orbiting around the “trapping circle” which is trapped orbit of χ constants near $v_{\parallel} \simeq V_R$ and $\psi \simeq 0$ in the (ψ, v_{\parallel}) space while nonresonant particles ($v_{\parallel} \not\simeq V_R$) move straightly parallel to the ψ axe (Figure 2 b). The resonant particles are pitch-angle scattered because of v_{\parallel} oscillation by orbiting the trapping circle, while the nonresonant particles are not pitch-angle scattered since v_{\parallel} of the particles are not changed. v_{\parallel} of resonant particles are changed from $v_{\parallel} \simeq V_R - V_t$ to $V_R + V_t$ within orbiting around the trapping circle, where resonant width V_t is,

$$V_t = \sqrt{\frac{\eta \Omega v_{\perp}}{k}}. \quad (10)$$

The resonant particles are orbiting around the trapping circle with trapping frequency Ω_t ,

$$\Omega_t = \sqrt{\eta \Omega k v_{\perp}}. \quad (11)$$

Due to these two constants, the pitch-angle scattering of resonant particles is constrained to a ε circle within $v_{\parallel} = V_R - V_t$ and $V_R + V_t$ (Figure 2 c). Resonant particles sense the wave phases from $\psi/\pi \simeq -0.5$ to 0.5 (Figure 2 b), which is corresponding to a half of all phases (2π). Therefore, the particles sense the wave phases corresponding to a half of wavelength in the real space (Figure 2 d).

Figure 3 shows the dispersion relation and the resonant lines ($\omega = kV_R + \Omega$) for protons and heavy ions in the 3 component plasma. The particles having $v_{\parallel} = V_R$ resonate with the waves on the crossing points where the resonant lines intersect the dispersion relation in the bottom of Figure 1. In the case of protons, particles resonate with two SBAs, which are Lp and Lh modes. In the case of heavy ions, particles resonate with the SPA (Lp mode) and

SBA (Lh mode). This fact leads heavy ions to the preferential heating. It is known that if two waves are counter-streaming with same speed exist, ε is not constant and the particles approximately move from one ε curve to another curve at random, which leads to the energy diffusion in the velocity space, the so-called the second order Fermi acceleration^{14,15}. In the case of protons, two SBAs are counter-streaming and have the about same speed, therefore resonant protons are understood as the second order Fermi acceleration. In the case of heavy ions, the SPA and SBA have very different wave speed and wavelength, thus resonant heavy ions experience a qualitative different acceleration mechanism from the case of the protons. In this thesis, we discuss that the resonance of the SPA plays an important role on the preferential heating of the heavy ions.

III. NUMERICAL STUDY

A. Simulation model

We consider a one-dimensional system with the main axis x . In the system, we suppose that there exist two waves with which protons (heavy ions) having $v_{\parallel} = V_A$ resonate. We choose α particles ($\Omega_h = \Omega_{\alpha} = \Omega_p/2$) as heavy ions. Given the two resonant waves, we integrate in time the Lorentz equation for ions,

$$m \frac{d\mathbf{v}}{dt} = q \left(\mathbf{E} + \frac{\mathbf{v}}{c} \times \mathbf{B} \right) ; \quad \frac{d\mathbf{r}}{dt} = \mathbf{v}, \quad (12)$$

where the electric and the magnetic fields are respectively given by $\mathbf{E} = (0, E_y, E_z)$, and $\mathbf{B} = (B_0, B_y, B_z)$, with

$$\begin{pmatrix} B_y \\ B_z \end{pmatrix} = \sum_{j=1}^2 B_{\perp,j} \begin{pmatrix} \sin(k_j x - \omega_j + \phi_j) \\ \cos(k_j x - \omega_j + \phi_j) \end{pmatrix} \quad (13)$$

and the transverse electric field is determined from $\mathbf{k} \times \mathbf{E} = \omega \mathbf{B}/c$, Faraday's law, where c is the speed of light. The following test particle discussion neglects the reaction of the particles on the waves. At first, we show the standard wave-particle interaction in the two coherent SBAs for protons. We study next the wave-particle interaction in the coherent SPA and SBA for heavy ions. The simulation parameters are as follows: we set $V_R = V_A$, then k and ω are determined so as to satisfy the resonant condition, $(\omega + \Omega)/k = V_R$. To specify the wave amplitudes, we assume that the two waves have the same Poynting flux. Faraday's law, $E_{\perp} = \{\omega/(ck)\}B_{\perp} = (V_{\text{ph}}/c)B_{\perp}$ where E_{\perp} is the wave amplitude of the electric field, requires the wave amplitudes η_{Lh} and η_{Lp} to satisfy $\eta_{Lh}^2 V_{\text{ph},Lh} = \eta_{Lp}^2 V_{\text{ph},Lp}$. The simulation parameters are given in Table I. The number of test particles n is 100,000, the initial velocities of test particles are $v_{\parallel} \simeq V_R = V_A$ and $v_{\perp} \sim 0$, the thermal velocity is $0.02V_A$ to the any direction. The initial positions are randomly distributed in space in order to have random phases with the wave.

Figure 2 shows the positions of the test particles in velocity space at $\Omega_p t = 100$ and the trajectory of a typical test particle from $\Omega_p t = 0$ to 100. In the case of run 1 which

is the simulation for the protons, the test particles diffuse across the constant ε curves of the two waves. In the case of run 2 which is the simulation for the heavy ions, however, the particles are not constrained to constant ε curves. They are efficiently heated in the perpendicular direction (note that the scale is not the same). This kind of particle motion cannot be explained in a conventional pitch angle diffusion model in a 2 component plasma. In the next subsections, we discuss more detail.

B. Result for protons

In this subsection, we discuss the result of run 1. Figure 4 (a) shows time evolution of v_{\perp} distribution for all test particles. The horizontal axis is time normalized by Ω_p^{-1} , the vertical axis is v_{\perp} normalized by V_A and color counter is the particle number density with a logarithm scale. As time goes on, particles are slowly diffused, and are heated up to $V_{\perp} \sim 3V_A$ in $100\Omega_p$. Figure 4 (b) shows time evolution of pitch-angle (the angle between the ambient field and particle velocity). We define the sign of the pitch-angle is positive when $v_{\parallel} > 0$ and is negative when $v_{\parallel} < 0$. The particles are quickly pitch-angle scattered. No particle have negative pitch angle because an initial v_{\parallel} is $+V_R$ and the particles are not strongly scattered to $v_{\parallel} < 0$. One can find a cyclic dense curve in Figure 4 (a) and (b). It means that some particles constrained to energy constant ε curves in one wave frame. There are also a dense lines extended to high v_{\perp} in Figure 4 (a), they are regarded as lucky particles in the sense that they are successively accelerated by resonating with two waves.

Figure 4 (c) shows time evolution of the phase angle (ψ) between v_{\perp} and B_{\perp} of the wave 1. The particles experience various phases. We turn the detail explanation to the next section, here we give a brief explanation with Figure 4 (d). A particle resonating with wave 1 (dense curve) senses the wave phases corresponding to a half of the wavelength of the wave 1 (λ_1), and the particle also experience various phases of the wave 2 (light curve) because waves 1 and 2 have similar wavelength, $\lambda_1 \simeq \lambda_2$. Therefore, particles experience various phases for both waves, and this fact leads that one can regard the particle motions to be

stochastic.

C. Result for heavy ions

In this subsection, we discuss a result of run 2. Figure 5 (a) shows time evolution of v_{\perp} distribution same as Figure 4 and theoretical result⁸ (dashed line), $v_{\perp} = \eta_{\text{SPA}} V_{\text{ph, SPA}} \Omega t$. The theory agrees very well with the simulation. The next section, we discuss the detail about the theory. Particles are “strongly” heated, which means that $\langle v_{\perp} \rangle$ (the average of v_{\perp} for all particles) linearly increases very faster than that in the case of run 1 (note that the scale of v_{\perp} of Figure 5 (a) is bigger than that of Figure 4 (a)) and the variance of v_{\perp} , $(1/n) \sum_j (v_{\perp,j} - \langle v_{\perp} \rangle)^2$ increase very slower than $\langle v_{\perp} \rangle$, where a subscript “ j ” denotes each particle. Figure 5 (b) shows time evolution of the pitch angle. The particles are quickly accelerated towards the perpendicular direction, and the particles are not pitch-angle scattered.

Figure 5 (c) shows time evolution for ψ_{SPA} , an angle between v_{\perp} and B_{\perp} of the SPA. Particles are very quickly “bunched” near $\psi_{\text{SPA}}/\pi \simeq 0.5$. The phase behavior is described by different terms, “phase trapping” and “phase bunching”. “Phase trapping” means a bounded phase oscillation of an individual resonant particle. On the other hand, “phase bunching” describes a state in which phases of many resonant particles are bunched around a certain wave phase¹². The time scale of the bunching is about Ω_p^{-1} . $\psi_{\text{SPA}}/\pi \simeq 0.5$ is the parallel to E_{\perp} of the SPA. Therefore, during the interaction most particles are always resonating with the SPA electric field and the particles are strongly heated to the direction to the electric field of the SPA, which is the perpendicular direction to the ambient magnetic field. On the other hand, other few particles are decelerated from $\Omega_p t \simeq 60$ (also see Figure 5 c), which are trapped only by the SPA and do not resonate with SBA. We turn the detail explanation to the next section, here we give a brief explanation with Figure 5 (d). A particle trapped by the SBA senses the wave phases corresponding to a half of the wavelength of the SBA, and the particle experiences a specific phase for the SPA (light curve)

because the SPA have very long wavelength than that of the SBA, $\lambda_{\text{SPA}} \gg \lambda_{\text{SBA}}$. During the trapping by short wave SBA, particles are bunched to the direction to the electric field of long wave SPA. Therefore the particles are strongly heated by experiencing the SPA electric field. This heating cannot be explained as the second ordered Fermi acceleration because of the specific phase bunching. The next section, we propose new heating model and obtain good agreement with the simulation result.

IV. THEORY

A. Explanation by ε and χ

In the case of run 1, two SBAs have about the same resonant width V_t . The top of Figure 6 is an illustration of typical particle motion in the velocity space, and the bottom of Figure 6 is that in (ψ, v_{\parallel}) space. We draw constant ε and V_t curves for two waves in the top of Figure 6, and the constant χ curves in Figure 6 (b). The particles are stochastically trapped by one of two waves, therefore the particles are sometimes trapped by one of two waves and sometimes trapped by another wave. Some particles are successively accelerated by resonating with two waves and some particles are decelerated by the two waves. Since fate of particles, accelerated or decelerated, is a matter of probability, the behavior of the particles becomes diffusive.

In the case of run 2, two waves have very different V_t , the SPA have larger V_t than that of the SBA. The top of Figure 7 is an illustration of typical particle motion in the velocity space, and the bottom of Figure 7 is that in (ψ, v_{\parallel}) space. The particles trapped by the SBA cannot orbit around the SPA trapping circle because v_{\parallel} of the particles are bounded within small variation by the χ constant curves of the SBA. Since the particles cannot orbit around the SPA trapping circle, thus ψ_{SPA} is not changed (Figure 7 bottom). The resonant particles are accelerated to the parallel direction only by B_{\perp} because the force of wave electric field E_{\perp} has the perpendicular direction. Because particles are trapped by a wave B_{\perp} varying v_{\parallel} to orbit around the trapping circle, the particles are trapped by the wave having stronger B_{\perp} . In the case of run 1, since B_{\perp} of two waves are about same, particles sometimes orbit around the trapping circle of one wave and sometimes orbit around that of another wave. On the other hand, in the case of run 2, $B_{\perp, \text{SBA}}$ is very greater than $B_{\perp, \text{SPA}}$. (Note that the SBA and SPA have same Poynting flux, $V_{\text{ph, SPA}} \eta_{\text{SPA}}^2 = V_{\text{ph, SBA}} \eta_{\text{SBA}}^2$, and $V_{\text{ph, SPA}} \gg V_{\text{ph, SBA}}$.) Therefore, most particles are orbiting around the trapping circle of the SBA. An important point is that SPA has larger trapping circle ($V_{t, \text{SPA}} > V_{t, \text{SBA}}$) though particles are trapped by the SBA

because the SBA has stronger magnetic field than that of the SPA ($B_{\perp,\text{SBA}} > B_{\perp,\text{SPA}}$). From the above discussions, we can get the conditions of the occurrence to the “strong” heating such as the case of run 2,

$$B_{\perp,\text{SPA}} < B_{\perp,\text{SBA}} \quad (14)$$

$$\lambda_{\text{SPA}} B_{\perp,\text{SPA}} > \lambda_{\text{SBA}} B_{\perp,\text{SBA}} \quad (15)$$

We examine Eqs. (14) and (15) by simulations in various parameters in Section V.

B. Purely electric and magnetic waves theory

In this subsection, we discuss about strong heating more quantitatively. In the case of run 2, the simulation for heavy ions, the SPA has a larger electric field and weaker magnetic field than the SBA since,

$$\frac{E_{\perp,\text{SBA}}}{E_{\perp,\text{SPA}}} = \frac{\eta_{\text{SBA}} V_{\text{ph,SBA}}}{\eta_{\text{SPA}} V_{\text{ph,SPA}}} \simeq 2, \quad (16)$$

$$\frac{B_{\perp,\text{SBA}}}{B_{\perp,\text{SPA}}} = \frac{\eta_{\text{SPA}}}{\eta_{\text{SBA}}} \simeq 0.2. \quad (17)$$

To simplify the discussion, we treat a model in which the SPA is taken as purely electric, while the SBA is assumed purely magnetic. We therefore neglect the magnetic field in the SPA and the electric field in the SBA. In other words, we treat “the purely electric wave” which brings only the electric field and “the purely magnetic wave” which has only the magnetic field. (These situations may be realized in the cut-off frequency with $k = 0$ and the resonance frequency with $k \rightarrow \infty$, respectively.) For propagation along the ambient magnetic field, the test particles obey the following equations of motion:

$$\frac{dv_{\parallel}}{dt} = \Omega\eta_B v_{\perp} \sin \psi_B, \quad (18)$$

$$\frac{dv_{\perp}}{dt} = \Omega(\eta_E c \cos \psi_E - \eta_B v_{\parallel} \sin \psi_B), \quad (19)$$

$$\begin{aligned} \frac{d\psi_B}{dt} &= -k_B(v_{\parallel} - V_R) \\ &\quad - \frac{\Omega}{v_{\perp}}(\eta_E c \sin \psi_E + \eta_B v_{\parallel} \cos \psi_B), \end{aligned} \quad (20)$$

$$\begin{aligned} \frac{d\psi_E}{dt} &= -k_E(v_{\parallel} - V_R) \\ &\quad - \frac{\Omega}{v_{\perp}}(\eta_E c \sin \psi_E + \eta_B v_{\parallel} \cos \psi_B), \end{aligned} \quad (21)$$

where $\eta_E = E_{\perp}/B_0$, $\eta_B = B_{\perp}/B_0$ (subscript “E” stands for the purely electric field and “B” describes the purely magnetic wave.)

Let us consider the case that only purely electric wave exists. Substituting $\eta_B = 0$ in Eqs.(18)-(21), these equations become

$$\frac{dv_{\parallel}}{dt} = 0, \quad (22)$$

$$\frac{dv_{\perp}}{dt} = A_E \cos \psi_E, \quad (23)$$

$$\frac{d\psi_E}{dt} = -k(v_{\parallel} - V_{R,E}) - \frac{A_E}{v_{\perp}} \sin \psi_E, \quad (24)$$

where we define a theoretical heating ratio, $A_E \equiv \eta_E \Omega c$. Eq.(22) indicates v_{\parallel} is a constant of time. We are interested in the behavior of resonant particles ($v_{\parallel} = V_R$). Eq.(24) becomes

$$\frac{d\psi_E}{dt} = -\frac{A_E}{v_{\perp}} \sin \psi_E, \quad (25)$$

showing that ψ_E decreases for $\psi_E > 0$ ($-\pi < \psi_E < \pi$), while ψ_E increases for $\psi_E < 0$. When $\psi_E \simeq 0$, v_{\perp} increases from Eq.(23) and $\dot{\psi}_E \rightarrow 0$ from Eq.(24). Therefore, ψ_E for resonant particles is approaching zero, reaching the stable equilibrium at $\psi_E = 0$. Resonant particles are quickly bunched to $\psi_E = 0$. The time scale of the particle to be bunched to $\psi_E = 0$ is

$$T_E = \frac{v_{\perp}}{A_E}. \quad (26)$$

In the case of run 2, T_E is given by

$$T_E \simeq \frac{v_{\perp}}{\eta_{\text{SPA}} \Omega V_{\text{ph,SPA}}} \simeq \Omega_p^{-1}, \quad (27)$$

where we use that because of Faraday's law $\eta_E c$ corresponds to $\eta_{SPA} V_{ph,SPA}$, and $v_{\perp} = 0.1V_A$ as a typical initial value. This indicates that the particles are immediately bunched at $\psi_E = 0$. Substituting $\psi_E = 0$ in Eq.(23) we have $v_{\perp} = A_E t$, with $v_{\perp} = 0$ initially. The resonant particle velocity increases linearly with the constant heating rate, A_E .

Next, let us consider the case that only purely magnetic wave exists. By substituting $\eta_E = 0$ in Eqs.(18)-(21), we obtain the constants of motion,

$$v_{\parallel}^2 + v_{\perp}^2 = \varepsilon \quad (28)$$

$$\frac{1}{2}(v_{\parallel} - V_R)^2 - \frac{\eta_B \Omega v_{\perp} \cos \psi_B}{k_B} \equiv \chi. \quad (29)$$

The purely magnetic wave has the same properties as the monochromatic wave. The resonant particles are trapped by the purely magnetic wave and are pitch-angle scattered. Because $\psi_B = 0$ of the center of the trapping circle, ψ_B oscillates near $\psi_B \simeq 0$.

Now, we discuss the case that both the purely electric wave and the purely magnetic wave coexist. We assume that v_{\parallel} is close to resonant velocity V_R . From the previous discussion, ψ_E becomes zero quickly and ψ_B oscillates near $\psi_B \simeq 0$. We discuss the particle motions having $\psi_E = 0$ and $\psi_B \ll 1$ after the initial time evolution. Furthermore, we assume $\eta_E c \gg \eta_B v_{\parallel} \psi_B$ because $\eta_{SPA} V_{ph,SPA} > \eta_{SBA} V_R$ in the case of run 2 ($\eta_E c$ corresponds to $\eta_{SPA} V_{ph,SPA}$, $\eta_{SBA} V_R \sim \eta_B v_{\parallel}$ and $\psi_B \ll 1$). We therefore neglect the second term of the right hand side in Eq.(19). We assume the particles have a large v_{\perp}/v_{\parallel} . Thus we can drop the last term of the right hand side in Eq.(21). In this approximation we finally get

$$v_{\parallel} = V_{t,B} \psi_{B0} \sin(\omega_{t,B} t) + V_R, \quad (30)$$

$$v_{\perp} = A_E t, \quad (31)$$

$$\psi_B = \psi_{B0} \cos(\omega_{t,B} t), \quad (32)$$

where $V_{t,B}$ is the trapping velocity for the purely magnetic wave, $V_{t,B} \equiv \sqrt{\eta_B \Omega v_{\perp} / k_B}$, $\omega_{t,B}$ is the trapping frequency for that, $\omega_{t,B} \equiv \sqrt{\eta_B \Omega v_{\perp} k_B}$ and ψ_{B0} is the initial value of ψ_B . These equations show that v_{\parallel} and ψ_B are determined by the purely magnetic wave and a simple harmonic oscillator while v_{\perp} is described by the purely electric wave alone and increases

linearly A_E . We have showed that (31) agree with the numerical result in the case of run 2 in Section III.

V. DEPENDENCE OF WAVE AMPLITUDES

A. Dependence of wave amplitudes for heavy ions

In this section, we perform simulations in various parameters of two waves in the case of run 2 (for heavy ions). In the previous sections, we assume that two waves have the same Poynting flux (Pf). Here, we study the dependence of the ratio of Poynting flux of two waves, Pf_{SPA}/Pf_{SBA} , and investigate the effect of the resonant velocity V_R . When V_R is changed, we must take different k and ω of two resonant waves (Figure 1 bottom). Thus the ratio of phase velocity, $V_{ph,SPA}/V_{ph,SBA}$ is also modified.

To decide whether strong heating occurs or does not for each simulation, we fit a numerical result on an equation,

$$\langle v_{\perp} \rangle = ct^{\alpha}, \quad (33)$$

where the bracket “ $\langle \rangle$ ” means an average for all particles. When the particles are strongly heated, one obtains $\alpha = 1$ from Eq.(31). On the other hand, when particles are only pitch-angle scattered, one obtains $\alpha = 0$ because pitch-angle scattering does not diffuse the particle energy (Eq.8). The top of Figure 8 shows an index α as the function of Pf_{SPA}/Pf_{SBA} and $V_{ph,SPA}/V_{ph,SBA}$. The horizontal and vertical axes are Pf_{SPA}/Pf_{SBA} and $V_{ph,SPA}/V_{ph,SBA}$, respectively. We execute simulations from $t\Omega_p = 0$ to 1000. We have confirmed that if the ratio of Poynting flux of two waves is same, the absolute value of Poynting flux does not affect the index α . The top of Figure 8 indicates that when the Poynting flux of two waves are same, the particles are strongly heated. When one of waves is weak, on the other hand, the particles are not heated, and then the particles are pitch-angle scattered by the wave having larger Poynting flux. The occurrence of the strong heating needs both of the SPA and SBA and the particles are not strongly heated even if which wave is missing. In the top of Figure 8, white hatched area is satisfied Eqs. (14) and (15), which agree very well with the numerical result. Therefore, we consider that Eqs. (14) and (15) are the necessary and sufficient conditions for the strong heating.

The bottom of Figure 8 shows a index c/A_E , where c means numerical heating ratio given by Eq. (33) only when $\alpha \simeq 1$ and A_E is theoretical heating ratio given by Eq. (31), respectively. In order to avoid misleading, we only plot c/A_E satisfying $\alpha > 0.9$ (the strong heating area) because c does not mean heating ratio when $\alpha \neq 1$, for example c means a constant velocity, $\langle v_\perp \rangle = c$ when $\alpha = 0$. In the left part ($Pf_{\text{SPA}}/Pf_{\text{SBA}} < 1$) of the strong heating area, one finds $c/A_E \simeq 1$ which means that theoretical result A_E agrees with numerical result c . On the other hand, one finds $c/A_E < 1$ in the right part of the strong heating area because some particles are strongly heated and others are only pitch-angle scattered. We discuss about this phenomenon in the following subsection.

B. Case of weak SPA

In this subsection, we discuss the case of $\lambda_{\text{SPA}} B_{\perp, \text{SPA}} \simeq \lambda_{\text{SBA}} B_{\perp, \text{SBA}}$, which is one of the critical parameter whether Eq.(15) is satisfied or not. In this case, the SPA has smaller Poynting flux than that of the SBA, that is to say, the SPA is weaker than the SBA. In the top of Figure 8, a white dashed curve on the left side is satisfied with $\lambda_{\text{SPA}} B_{\perp, \text{SPA}} = \lambda_{\text{SBA}} B_{\perp, \text{SBA}}$. Here, we take $V_{\text{ph,SPA}}/V_{\text{ph,SBA}} = 21.7$ and $Pf_{\text{SPA}}/Pf_{\text{SBA}} = 0.098$ (black circle in the top of Figure 8). The top of Figure 9 shows time evolution of v_\perp from $t\Omega = 0$ to 1000, and the white dashed line is the theoretical heating ratio (Eq.31). Before $t\Omega \simeq 200$, particles are heated same as theory, but the after, the particles are not strongly heated. The bottom of Figure 9 is an illustration of a typical particle motion in (ψ, v_\parallel) space. In this case, the resonant width of the SPA, $V_{t, \text{SPA}}$ is same as $V_{t, \text{SBA}}$. At first, the particles are trapped by the SBA and phases for the SPA are bunched at $E_{\perp, \text{SPA}}$, thus the particles are strongly heated. However, the phase bunching for the SPA is gradually broken because by orbiting around the trapping circle of the SBA the particles can easily obtain v_\parallel enough to orbit around the trapping circle of the SPA (note $V_{t, \text{SBA}} \simeq V_{t, \text{SPA}}$). The SPA is not strong enough to bunch the particles at the direction of the electric field of the SPA. Therefore, the particles gradually drop out of the strong heating process.

C. Case of strong SPA

We discuss the case of $B_{\perp,SPA} \simeq B_{\perp,SBA}$, which is another critical parameter whether Eq.(14) is satisfied or not. In this case, the SPA has bigger Poynting flux than that of the SBA, that is to say, the SPA is stronger than the SBA. In the top of Figure 8, a white dashed line on the right side is satisfied with $B_{\perp,SPA} \simeq B_{\perp,SBA}$. Here, we take $V_{ph,SPA}/V_{ph,SBA} = 21.7$ (same as previous subsection) and $Pf_{SPA}/Pf_{SBA} = 20.5$ (black square in the top of Figure 8). The top of Figure 10 shows time evolution of v_{\perp} from $t\Omega = 0$ to 1000. Most particles are pitch-angle scattered and energy diffused slowly. The frequency of these pitch-angle scattering indicates that the particles resonate with the SPA. However, some particles are strongly heated and their heating ratio agrees with the theoretical heating ratio (not shown). Some particles begin to be strongly heated, and once the heating begins, the particles never drop out of the strong heating process. The bottom of Figure 10 is an illustration of a typical particle motion in (ψ, v_{\parallel}) space. In this case, some particles orbit around the trapping circle of the SPA because the magnetic field of the SPA is strong as same as that of the SBA, and particles moves neglecting χ counters for the SBA. Therefore, they are pitch-angle scatted by the SPA. However, some particles are sometimes trapped by the SBA, and begin to be phase-bunched near $E_{\perp,SPA}$. Such particles never orbit around the trapping circle of the SPA again because the particles trapped by the SBA cannot obtain v_{\parallel} enough (note $V_{t,SPA} \gg V_{t,SBA}$). Therefore, the selected particles are strongly heated all the time after the selection. Let us see the top of Figure 10 again, most particles begin to be strongly heated at $v_{\perp} \simeq 0$. The time scale of the particle to be bunched at $\psi_{SPA} = 0$ is given by Eq.(26). When v_{\perp} is small, particles are rapidly bunched at $\psi_{SPA} = 0$ and easily begin to be strongly heating. Therefore, particles are selected every trapping frequency of the SPA and make lines at equal intervals in the top of Figure 10.

D. Dependence of wave amplitudes for protons

We also perform simulations in various parameters of two waves in the case of run 1 (for protons). The top of Figure 11 shows the index α in the same format as Figure 8. The strong heating area is very narrower than that in the case of heavy ions. The bottom of Figure 11 shows the index c/A_E in the case of protons. Protons are strongly heated only when the wave parameters are very specific. Note that the scale of vertical axis is not same as Figure 8 because the protons cannot resonate with two wave having very different wavelength (Figure 1 bottom). Therefore, very specific wave parameters are satisfied with Eqs. (14) and (15). We consider that the strong heating occurs not only for the heavy ions but also for the protons. The conditions Eqs.(14),(15) are satisfied for protons only when waves have the specific amplitudes because the protons cannot resonate with two waves having very different wavelength while these conditions can be easily satisfied for the heavy ions in the 3 component plasma because the SPA having very long wavelength exists.

E. Dependence of wave amplitudes in the 2 component plasma

We also perform simulations in various parameters for protons in the 2 component plasma. In the 2 component plasma, there are whistler and EMIC modes (Figure 1 top). We account the index α in various parameters in the coherent whistler and EMIC waves resonating with the protons. Figure 12 shows the index α in the same format as Figure 8 except the vertical axis is V_R . This result shows that the protons are strongly heated even in the 2 component plasma when two waves have specific parameters. The top of Figure 13 shows v_{\perp} at $Pf_{\text{EMIC}}/Pf_{\text{Whistler}} = 0.26$ and $V_R = 3$ (black circle in Figure 12). Some particles are strongly heated and others are pitch-angle scattered, it is similar to the case of the strong SPA in the previous subsection. In this case, it is different from the case of the SPA and SBA that the EMIC has longer wavelength and weaker electric field (slower phase velocity) than the whistler wave while the SPA has longer wavelength and stronger electric field than that

of the SBA. The heating ratio obtained by numerical result for selected particles agrees with theoretical heating ratio obtained by whistler electric field, and the strength of EMIC electric field is too weak to explain the numerical heating ratio. However, the selected particles not may be bunched to the direction of the whistler electric field (Figure 13 bottom, the direction of wave electric field is $\psi_{\text{Whistler}}/\pi = 0.5$), and the particles are buched at $\psi_{\text{Whistler}}/\pi \simeq 0.2$. It may not be easy to explain the reason.

VI. SUMMARY AND DISCUSSION

We have discussed a new heating process of heavy ions in two coherent EMIC waves having different wavelength each other by using the test particle simulations, and we have proposed the new models which agree with simulations. We have found that particles are strongly heated in the two coherent circularly polarized waves which are satisfied

$$B_{\perp,1} < B_{\perp,2}, \quad (34)$$

$$\lambda_1 B_{\perp,1} > \lambda_2 B_{\perp,2}, \quad (35)$$

and the heating ratio for the perpendicular direction to the ambient magnetic field, A_E is

$$A_E = \frac{B_{\perp,1}}{B_0} \frac{\omega_1}{k_1} \Omega, \quad (36)$$

where subscript “1” and “2” describe one of two coherent waves and wave 1 is longer than wave 2 ($k_1 < k_2$). The above conditions can be easily satisfied for the heavy ions in the 3 component plasma, because the cut-off EMIC wave which has very long wavelength exists. On the other hand, it is difficult that the above conditions are be satisfied for protons, because the protons cannot resonate with the two waves which have very different wavelength. Therefore, heavy ions are strongly heated within various wave parameters while protons are heated within specific parameters. The dispersion relation in the 3 component plasma leads to such preferential heating of heavy ions.

We assumed for simplicity two coherent waves model, but we expect that heavy ions are strongly heated in one coherent long wave and weak turbulence, and if that is right, the model proposed by this thesis will take more applications to heliospheric and astronomical phenomena. Now, we are analyzing about this issue. We did not discuss how a coherent long EMIC wave is excited. One of the possible processes is an anisotropic thermal α particle beam instability¹⁰. Other possible process is a parametric instability in the multi component plasma⁹. The excitation mechanisms of this mode should be studied further. We are also planning to study the self-consistent interaction between waves and particles using a hybrid simulation.

We have only begun to investigate the potentially rich particle heating process in the multi-component plasma. It is important to study our theoretical model from other aspects such as the stochastic/chaotic heating process etc.^{16,17}. This issue will be reported elsewhere.

We expect that this theory can be applied to many heliospheric and astronomical phenomena. In future publications, we hope to show that observed preferential heating agrees with new heating model proposed in this thesis.

REFERENCES

- ¹ S. R. Cranmer, J. L. Kohl, G. Noci, E. Antonucci, G. Tondello, M. C. E. Huber, L. Strachan, A. V. Panasyuk, L. D. Gardner, M. Romoli, S. Fineschi, D. Dobrzycka, J. C. Raymond, P. Nicolosi, O. H. W. Siegmund, D. Spadaro, C. Benna, A. Ciaravella, S. Giordano, S. R. Habbal, M. Karovska, X. Li, R. Martin, J. G. Michels, A. Modigliani, G. Naletto, R. H. O’Neal, C. Pernechele, G. Poletto, P. L. Smith, and R. M. Suleiman, *Astrophys. J.* **511**, 481, (1999).
- ² E. J. Lund, E. Möbius, L. Tang, L. M. Kistler, M. A. Popecki, D. M. Klumpar, W. K. Peterson, E. G. Shelley, B. Klecker, D. Hovestadt, M. Temerin, R. E. Ergun, J. P. McFadden, C. W. Carlson, F. S. Mozer, R. C. Elphic, R. J. Strangeway, C. A. Cattell, and R. F. Pfaff, *Geophys. Res. Lett.* **25**, 2049 (1998).
- ³ R. E. Erlandson, L. J. Zanetti, M. H. Acuña, A. I. Eriksson, L. Eliasson, M. H. Boehm, and L. G. Blomberg, *Geophys. Res. Lett.* **21**, 1855 (1994).
- ⁴ M. Tanaka, *J. Geophys. Res.* **90**, 6459 (1985).
- ⁵ C. F. Kennel and F. Engelmann, *Phys. Fluids* **9** 2377 (1966).
- ⁶ V. K. Jordanova, J. U. Kozyra, and A. F. Nagy, *J. Geophys. Res.* **101**, 19771 (1996).
- ⁷ P. A. Isenberg, *Space Sci. Rev.* **95**, 119 (2001).
- ⁸ T. Mizuta and M. Hoshino, *Geophys. Res. Lett.* **28**, 3099 (2001).
- ⁹ T. Kubo, master thesis, University of Tokyo (1986).
- ¹⁰ K. Killen, N. Omid, D. Krauss-Varban, and H. Karimabadi, *J. Geophys. Res.* **100**, 5835 (1995).
- ¹¹ S. P. Gary, L. Yin, D. Winske, and D. B. Rsisenfeld, *J. Geophys. Res.* **105**, 20989 (2000).
- ¹² H. Matsumoto, *Wave Instabilities in Space Plasmas*, D. Reidel Pub. Co. **74**, 163 (1979).

- ¹³ M. Hoshino and T. Terasawa, *J. Geophys. Res.* **90**, 57 (1985).
- ¹⁴ T. Terasawa, *Geophysical Monograph*, American Geophysical Union, **53**, 41 (1989).
- ¹⁵ T. Sugiyama, M. Fujimoto, and T. Mukai, *J. Geophys. Res.* **106**, 21657 (2001).
- ¹⁶ W. Horton and Y. H. Ichikawa, *Chaos and Structures in Nonlinear Plasmas*, World Scientific Pub. Co. (1996).
- ¹⁷ R. White, L. Chen and Z. Lin, *Phys. Plasmas* (in press).

TABLES

TABLE I. Parameters for the test particle simulations

run	particles	wave 1	wave 2
1	protons	SBA ($B_{\perp}/B_0 = 0.075, V_{\text{ph}}/V_A \simeq -1.2$)	SBA ($B_{\perp}/B_0 = 0.1, V_{\text{ph}}/V_A \simeq -0.68$)
2	heavy ions (α)	SPA ($B_{\perp}/B_0 = 0.022, V_{\text{ph}}/V_A \simeq 18$)	SBA ($B_{\perp}/B_0 = 0.1, V_{\text{ph}}/V_A \simeq -0.83$)

FIGURES

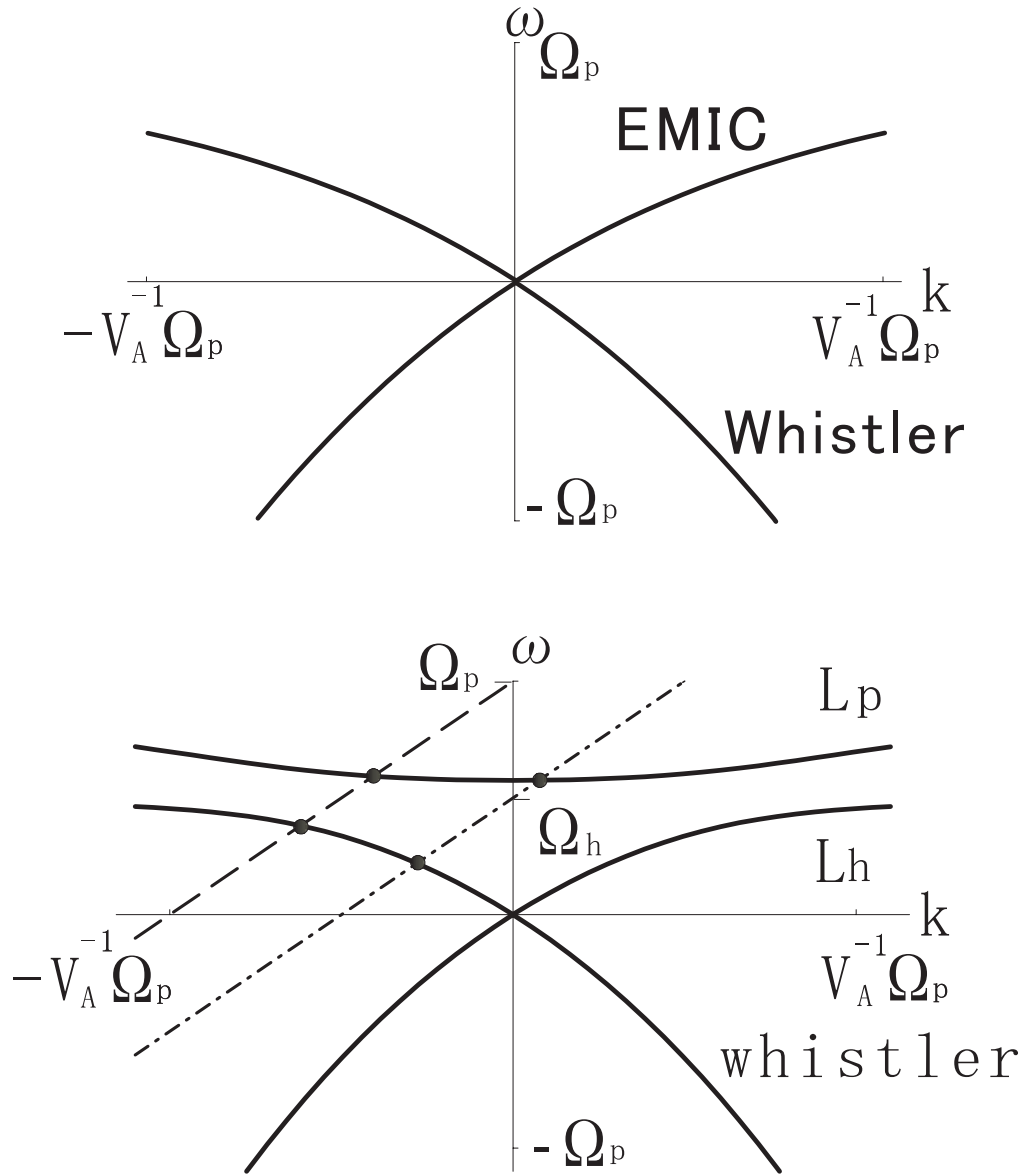


FIG. 1. The dispersion relation in 2 component plasma (top) and in 3 component plasma (bottom), the solid lines are the dispersion relations, and the dashed line is the resonance line for heavy ions (α particles) and the dot-dashed line for protons.

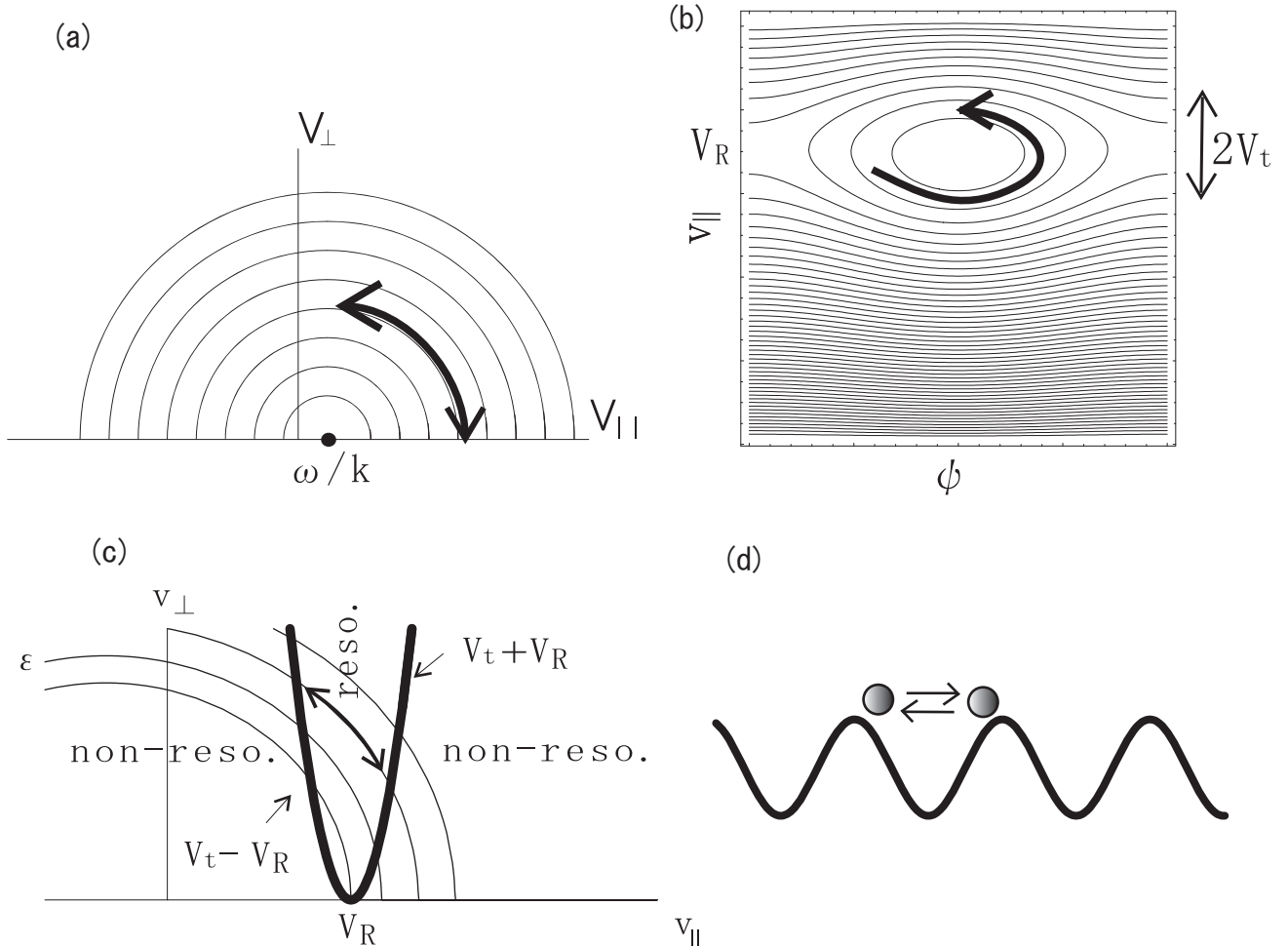


FIG. 2. (a): Constant ε circles in $(v_{\parallel}, v_{\perp})$ space. ε means the energy conversation in the wave frame. The particle motions are constrained to a constant ε circle. The arrow shows a typical particle trajectory in this space. (b): Constant χ curves in (ψ, v_{\parallel}) space. The arrow shows the trajectory of a typical resonant particle in this space. (c): An arrow is the trajectory of a typical resonant particle motion in $(v_{\parallel}, v_{\perp})$ space. We also draw constants ε (thin solid circles) and resonant width (thick solid curves). The pitch-angle scattering of resonant particles is constrained to a ε circle from $v_{\parallel} = V_R - V_t$ to $V_R + V_t$. (d): An illustration of the resonant particle motion in one coherent wave in the real space. A resonant particle senses the wave phases corresponding to a half of wavelength in one coherent wave.

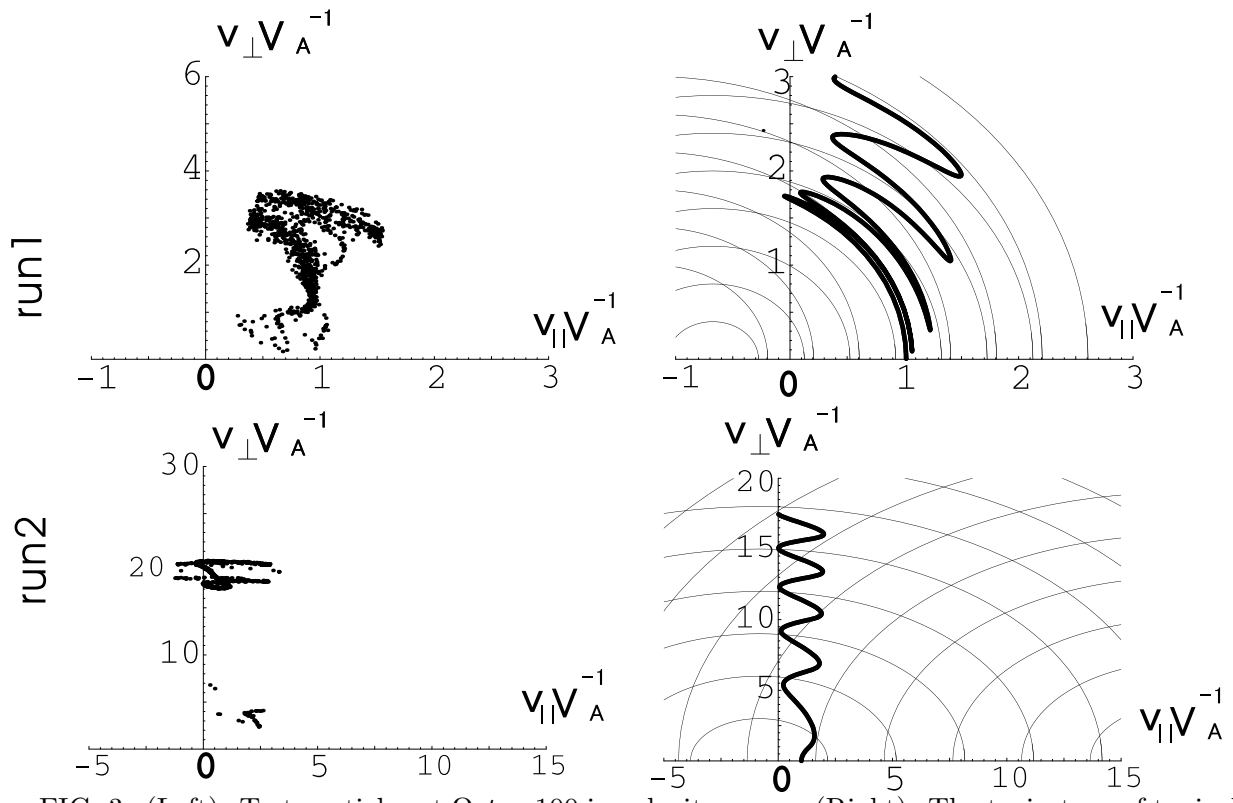


FIG. 3. (Left): Test particles at $\Omega_p t = 100$ in velocity space. (Right): The trajectory of typical test particle (solid lines) and ε constant curves by two waves (thin curves) in the velocity space. Top is for run 1 (protons) and bottom is for run 2 (heavy ions).

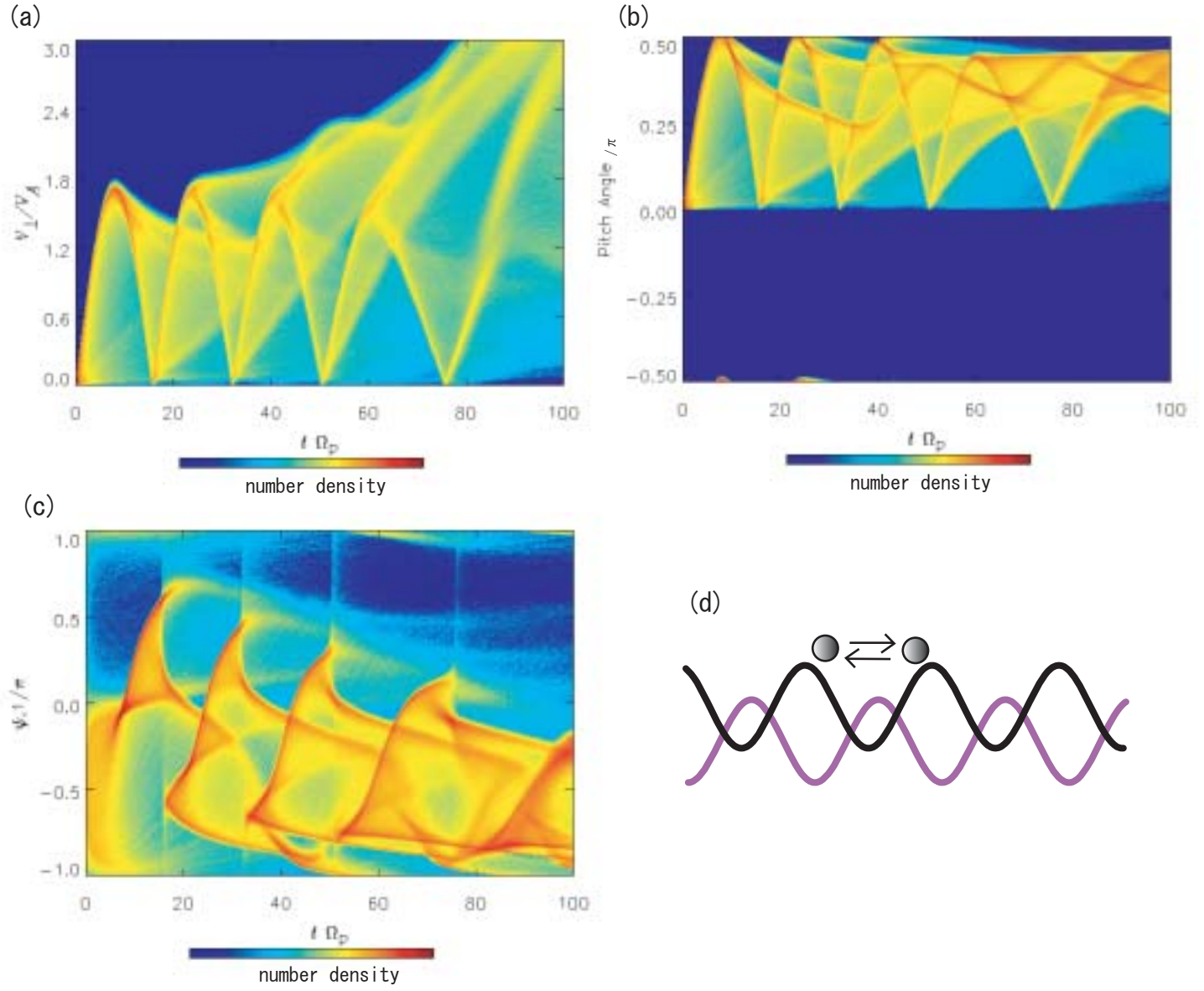


FIG. 4. The time evolution of v_{\perp} (a), the pitch angle (the angle between the ambient field and particle velocity) (b) and the phase angle (ψ) between v_{\perp} and B_{\perp} of the wave 1 (c) for all test particles in the case of run 1 (for protons). The horizontal axis is time normalized by Ω_p^{-1} , the vertical axis is v_{\perp} normalized by V_A and color counter is the particle number density with a logarithm scale. We define the sign of the pitch-angle is positive when $v_{\parallel} > 0$ and is negative when $v_{\parallel} < 0$. (d): An illustration of the resonant particle motion in the two coherent SBAs in the real space in the case of run 1 (for protons). The resonant particle trapped by the wave 1 experiences various phases of the wave 2 and one can regard the particle motions as stochastic.

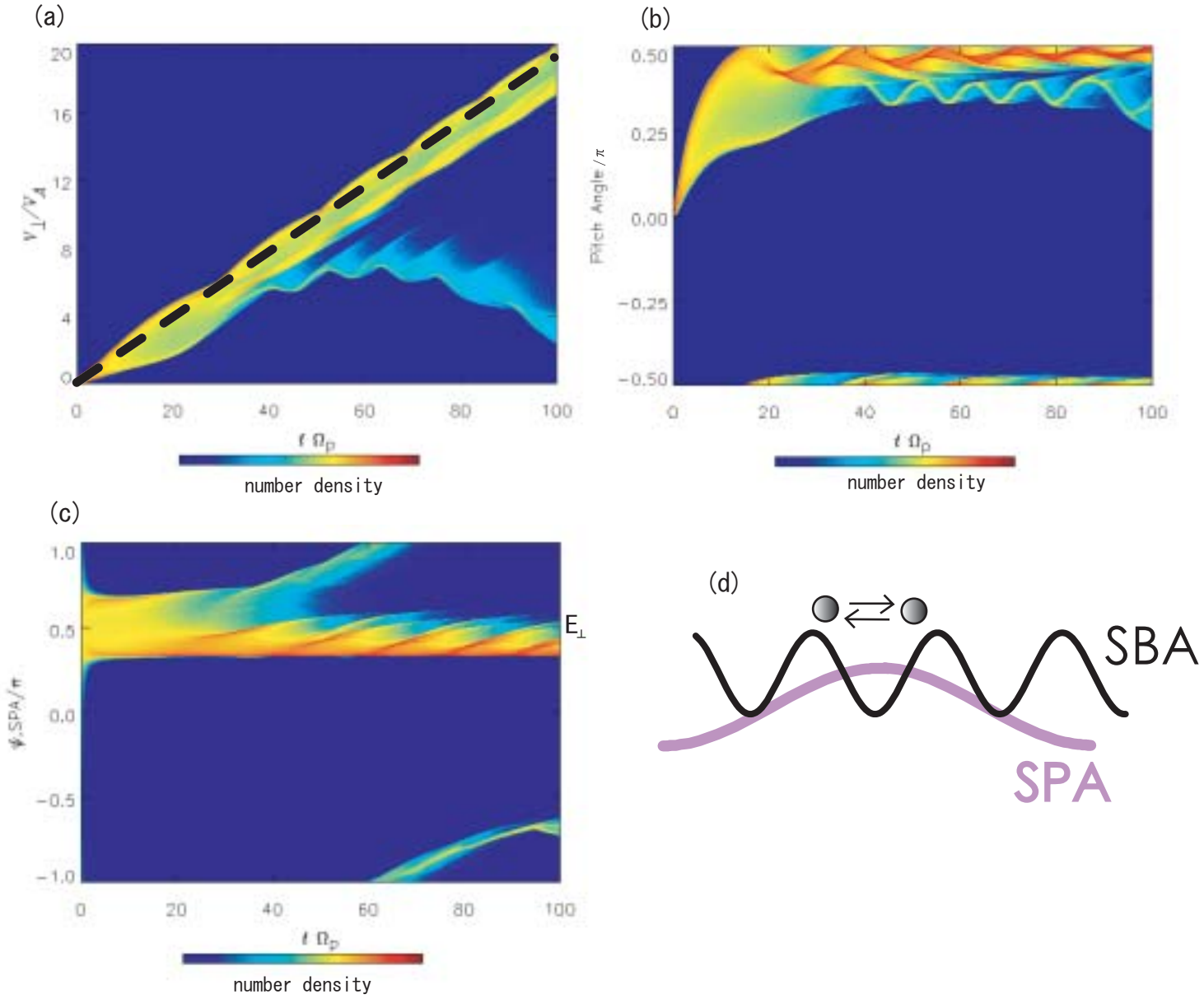


FIG. 5. The time evolution of v_{\perp} distribution and theoretical result (dashed line) (a), the pitch angle (b), and ψ_{SPA} , an angle between v_{\perp} and B_{\perp} of the SPA (c) in the case of run 2 (for heavy ions). (d): An illustration of the resonant particle motion in the coherent SPA (thin curve) and SBA (dense curve) in the real space in the case of run 2 (heavy ions). Within the resonant particle being trapped by short wave SBA, the particle always experiences the specific phase of the SPA.

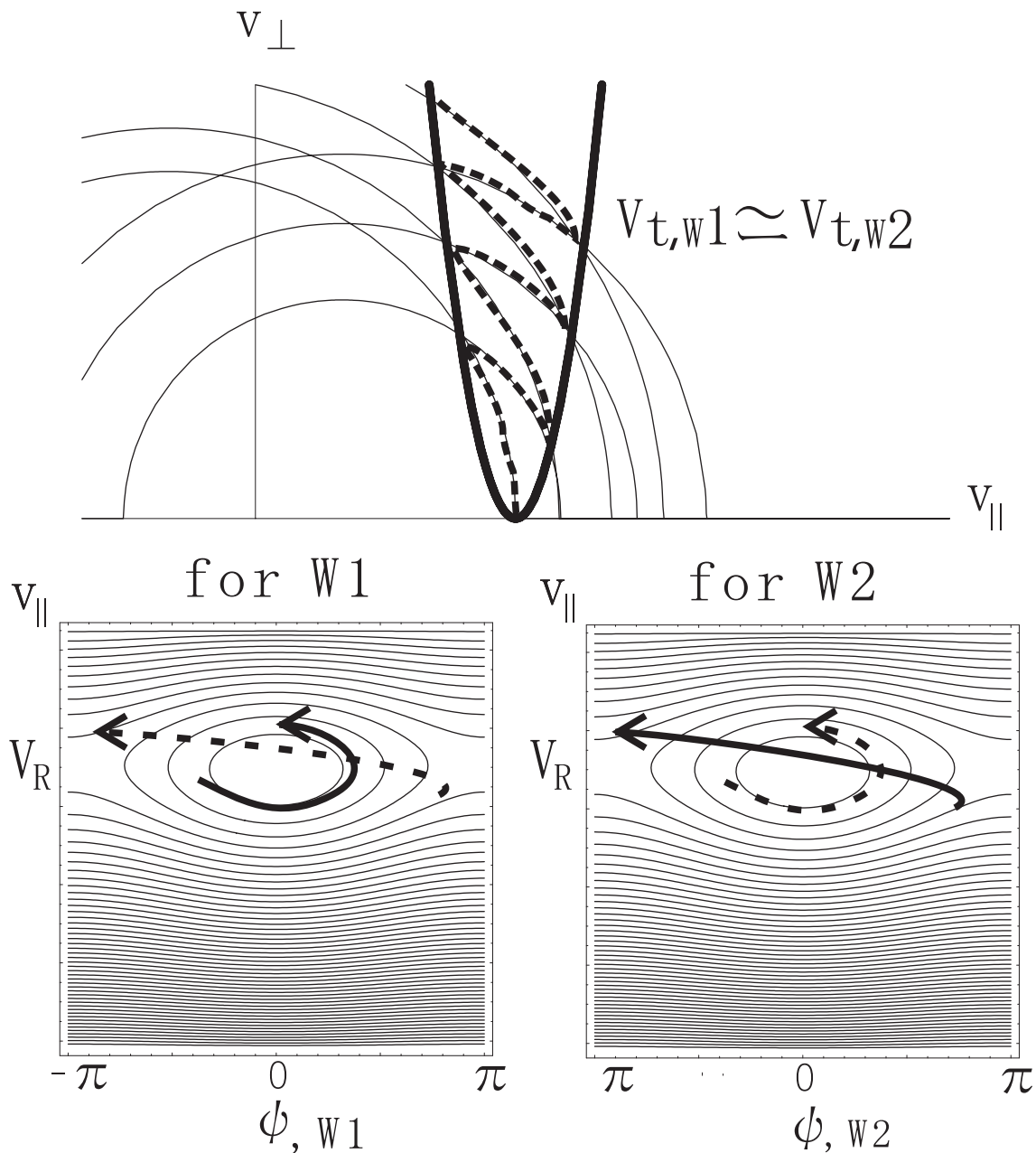


FIG. 6. An illustration of typical particle motion (dashed curve) in the velocity space (top) and in the (ψ, v_{\parallel}) space (bottom) in the case of run 1 (for protons). We also draw constants ε curves (thin solid circles) and resonant width (thick solid curves) on the top panel. A particle is sometimes trapped by one of two waves and is sometimes trapped by another wave.

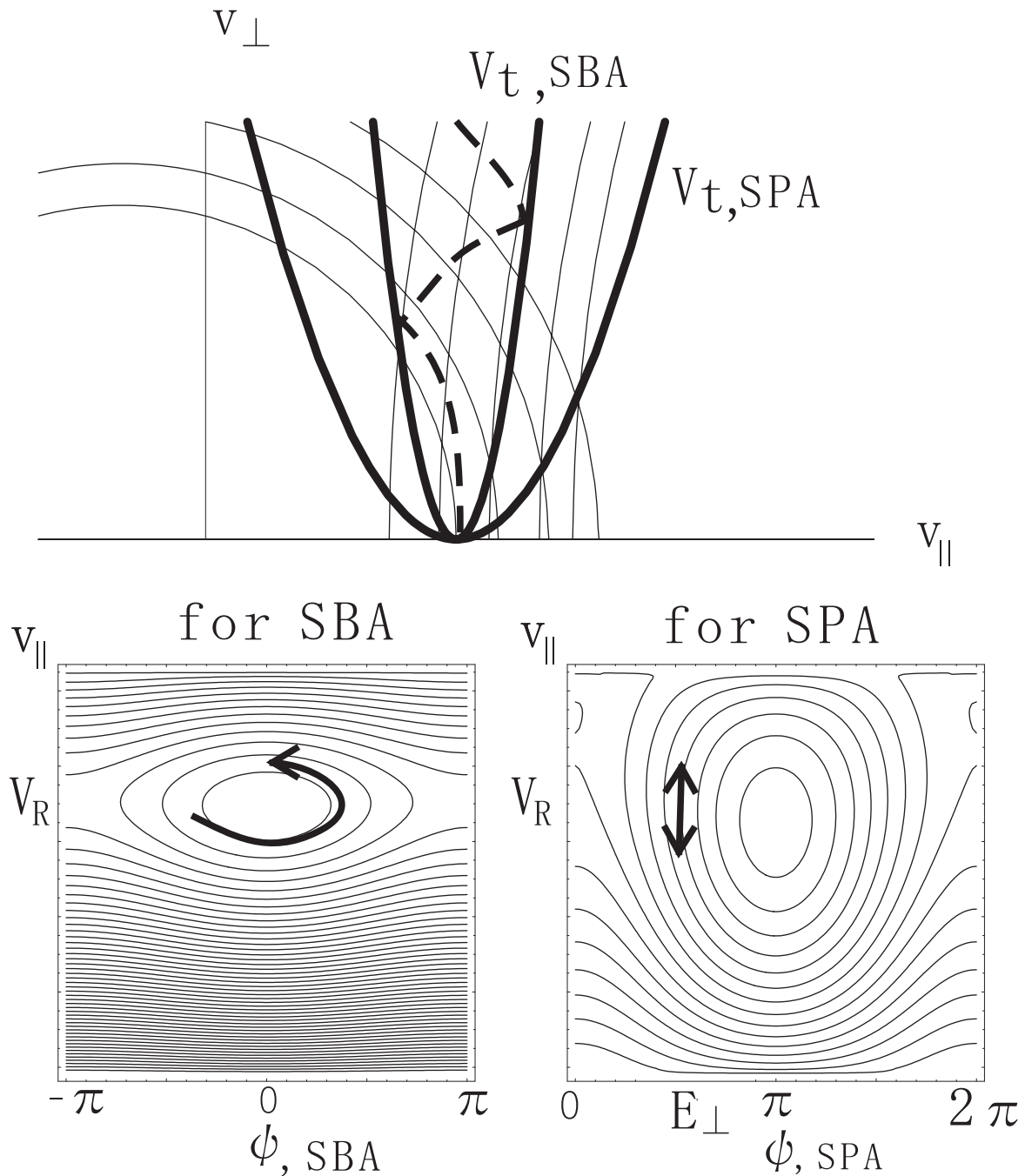


FIG. 7. An illustration of typical particle motion (dashed curve) in the velocity space (top) and in the (ψ, v_{\parallel}) space (bottom) in the case of run 2 (for heavy ions). We also draw constants ε curves (thin solid circles) and resonant width (thick solid curves) on the top panel. The resonant particle trapped by the SBA cannot orbit around the trapping circle of the SPA because the particles cannot obtain the varying of v_{\parallel} enough to orbit around the trapping circle of the SPA, therefore ψ_{SPA} is not changed.

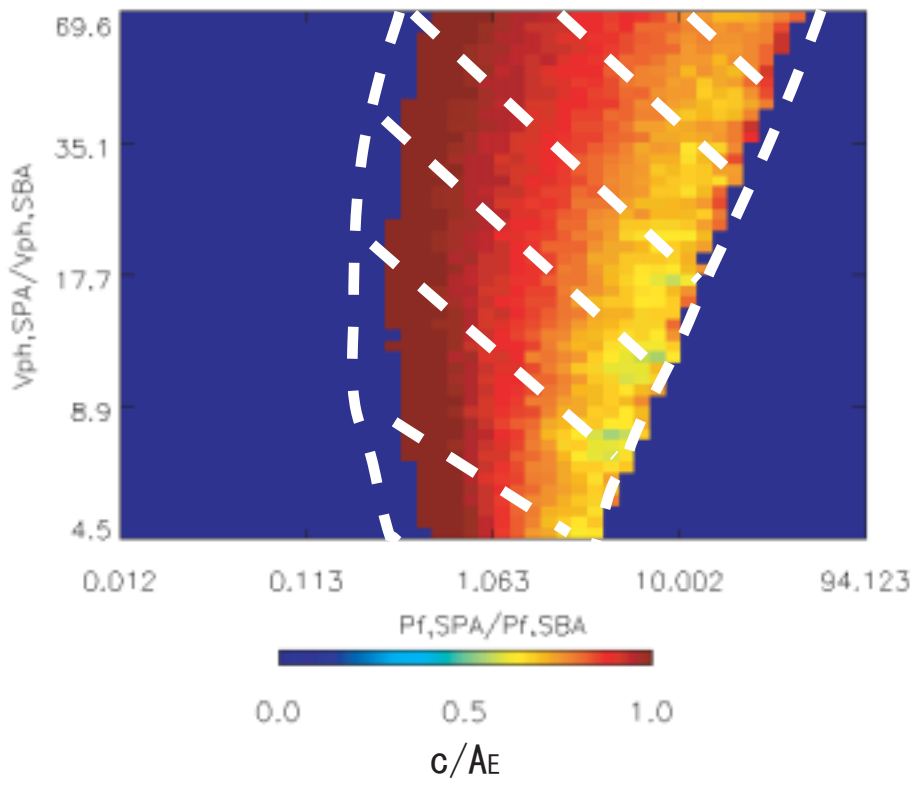
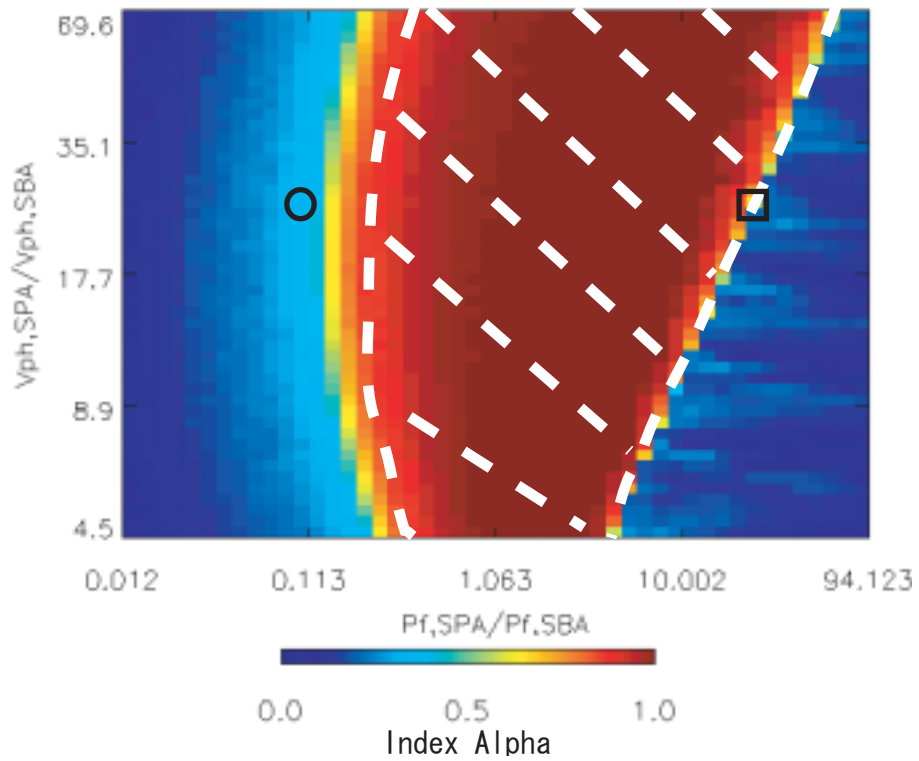


FIG. 8. (a): The index α (color) obtained from a fitting equation, $\langle v_{\perp} \rangle = ct^{\alpha}$ ($t\Omega_p = 0 \rightarrow 1000$) in various parameters of two waves in the case of heavy ions. The horizontal and vertical axes are $Pf_{\text{SPA}}/Pf_{\text{SBA}}$ and $V_{\text{ph,SPA}}/V_{\text{ph,SBA}}$, respectively. White hatched area enclosed white dashed curves is the strong heating area obtained by the theory discussion in Section IV. We also perform case studies, the case of weak SPA, $\lambda_{\text{SPA}}B_{\perp,\text{SPA}} \simeq \lambda_{\text{SBA}}B_{\perp,\text{SBA}}$ (black circle) and the case of strong SPA, $B_{\perp,\text{SPA}} \simeq B_{\perp,\text{SBA}}$ (a black square). (b): The index c/A_E in the case of heavy ions, where c means numerical heating ratio given by $\langle v_{\perp} \rangle = ct^{\alpha}$ and A_E is theoretical heating ratio. In order to avoid misleading, we only plot c/A_E satisfying $\alpha > 0.9$ (the strong heating region) because c does not mean heating ratio when $\alpha \neq 1$, for example c means a constant velocity, $\langle v_{\perp} \rangle = c$ when $\alpha = 0$. White dashed curves are same as (a)

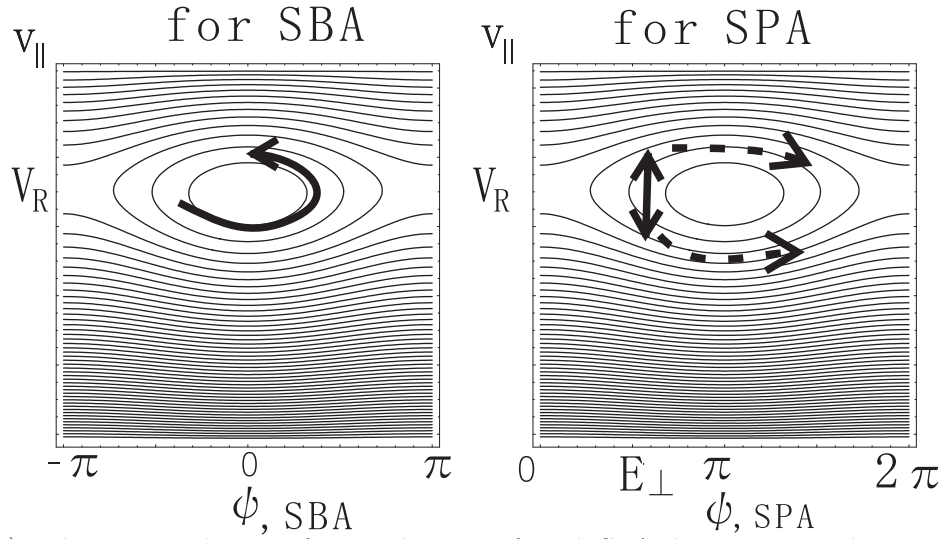
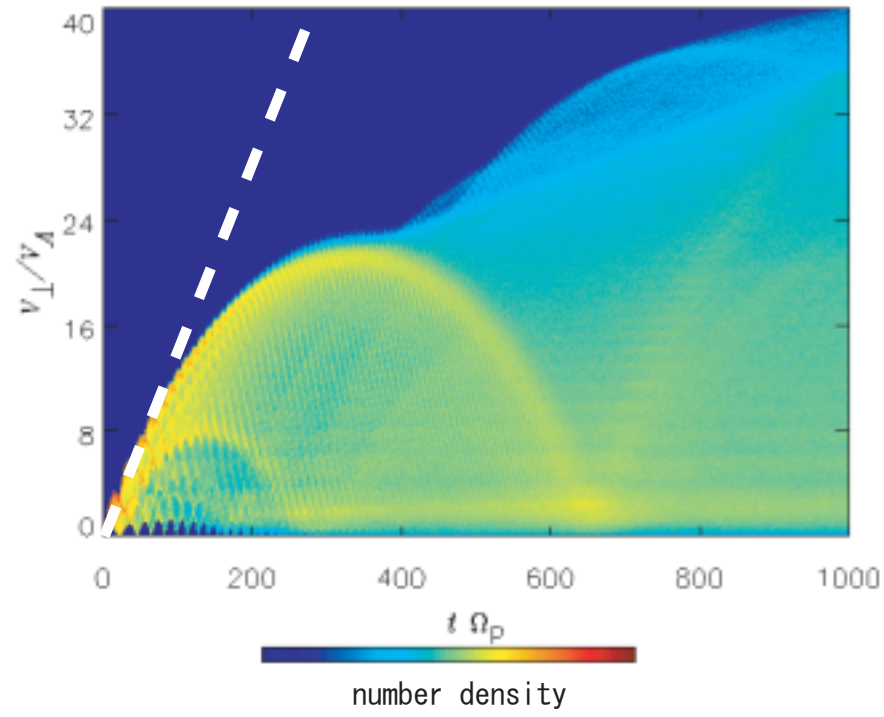


FIG. 9. (a): The time evolution of v_{\perp} in the case of weak SPA, $\lambda_{\text{SPA}} B_{\perp, \text{SPA}} \simeq \lambda_{\text{SBA}} B_{\perp, \text{SBA}}$ (black circle in Figure 8). White dashed line is the theoretical heating ratio. (b): An illustration of a typical particle motion in (ψ, v_{\parallel}) space.

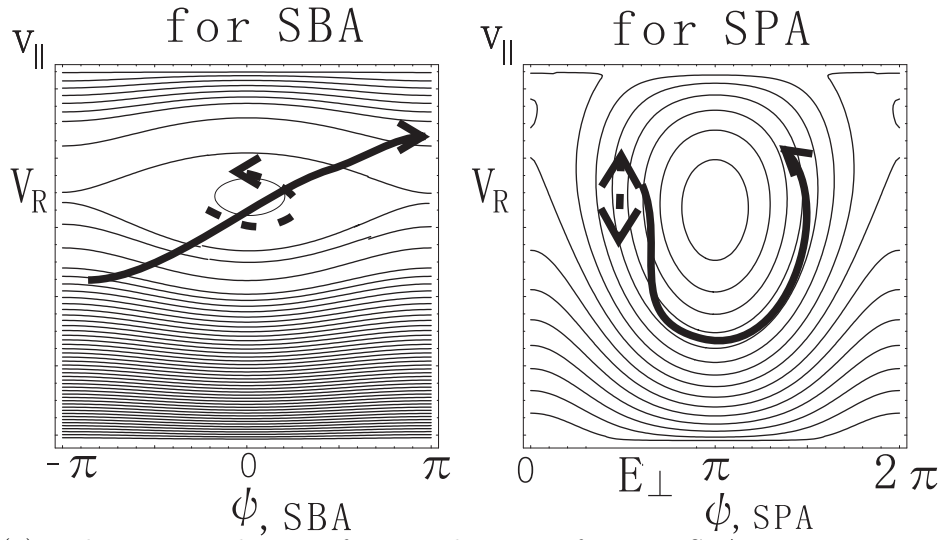
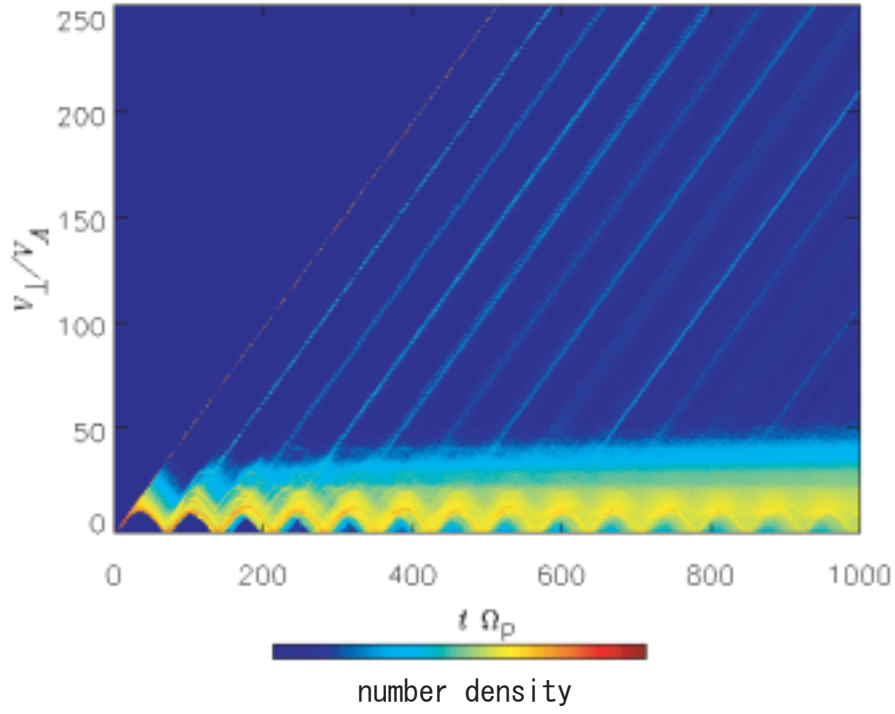


FIG. 10. (a): The time evolution of v_{\perp} in the case of strong SPA, $B_{\perp,SPA} \simeq B_{\perp,SBA}$ (black square in Figure 8). (b): An illustration of a typical particle motion in (ψ, v_{\parallel}) space.

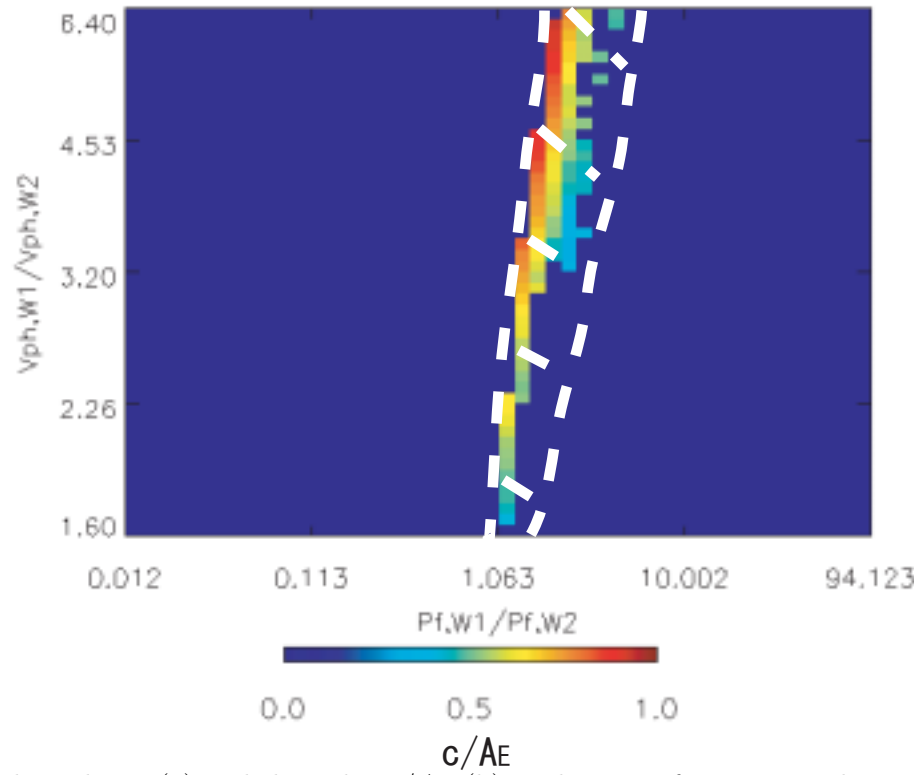
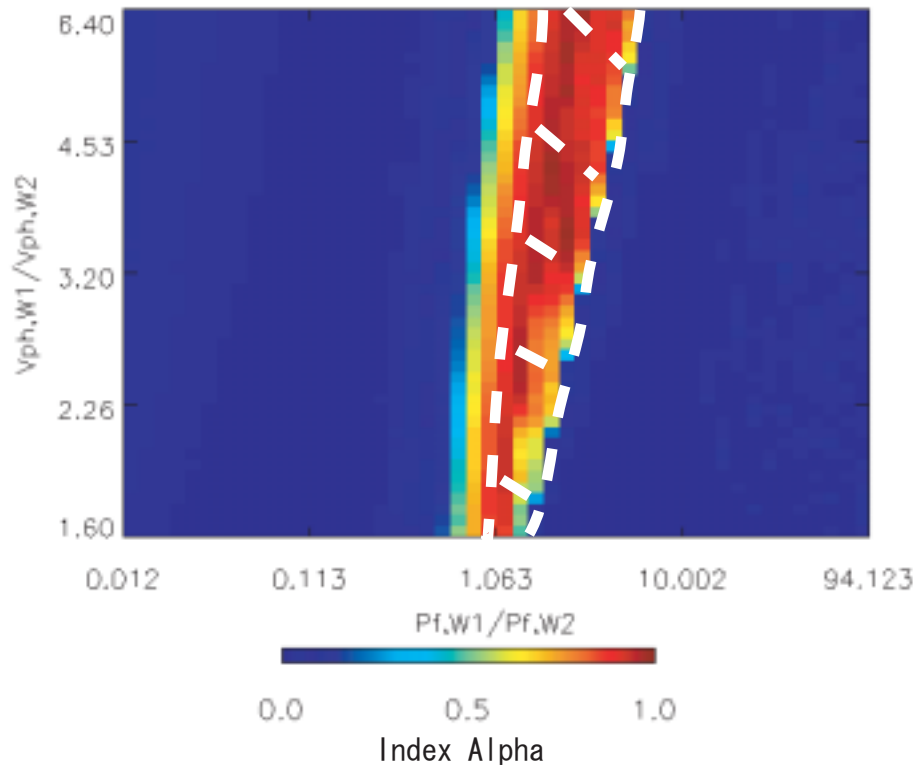


FIG. 11. The index α (a) and the index c/A_E (b) in the case of protons in the same format as Figure 8.

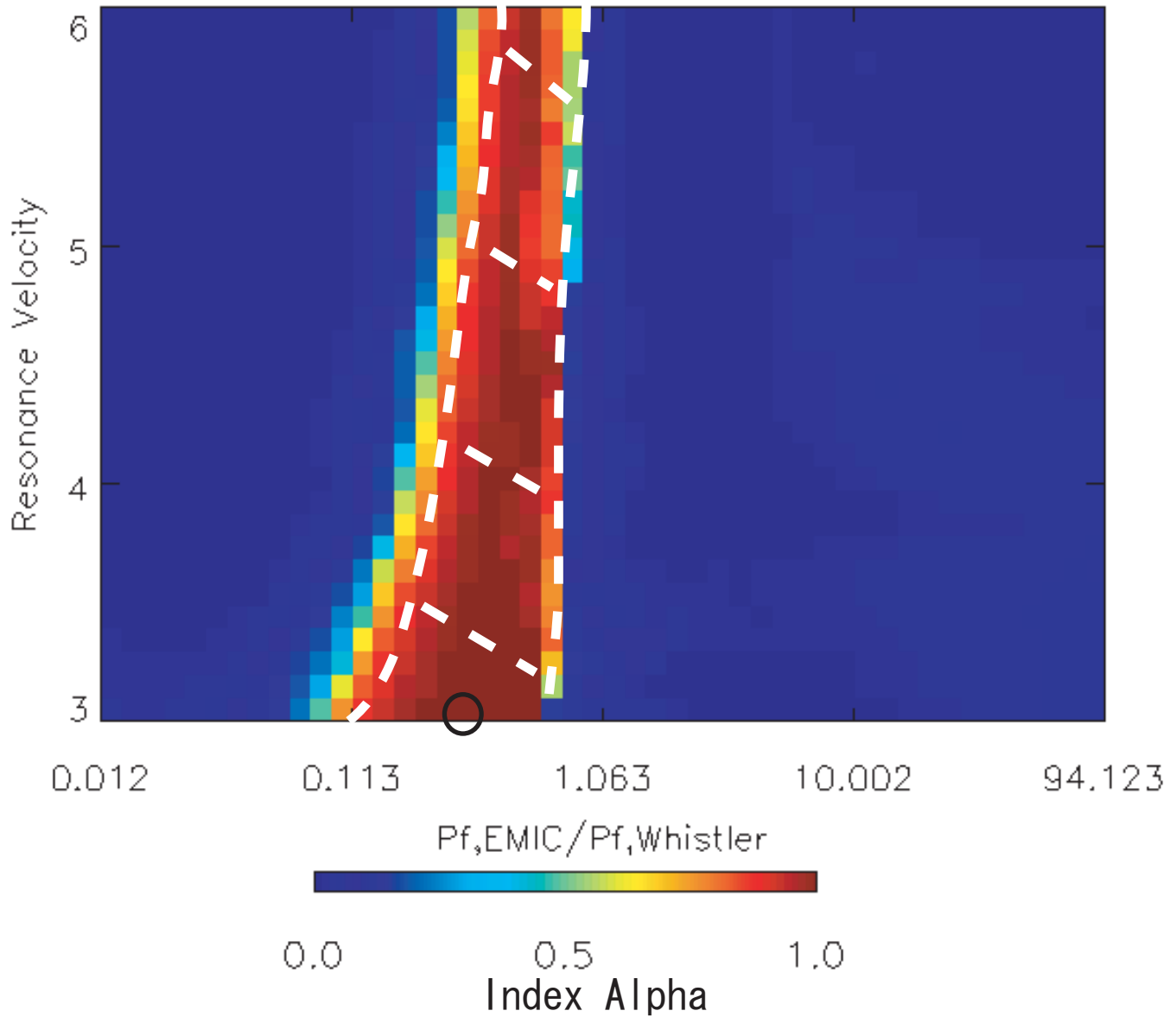


FIG. 12. The index α in the case of the 2 component plasma in the same format as Figure 8 except the vertical axe is the resonant velocity.

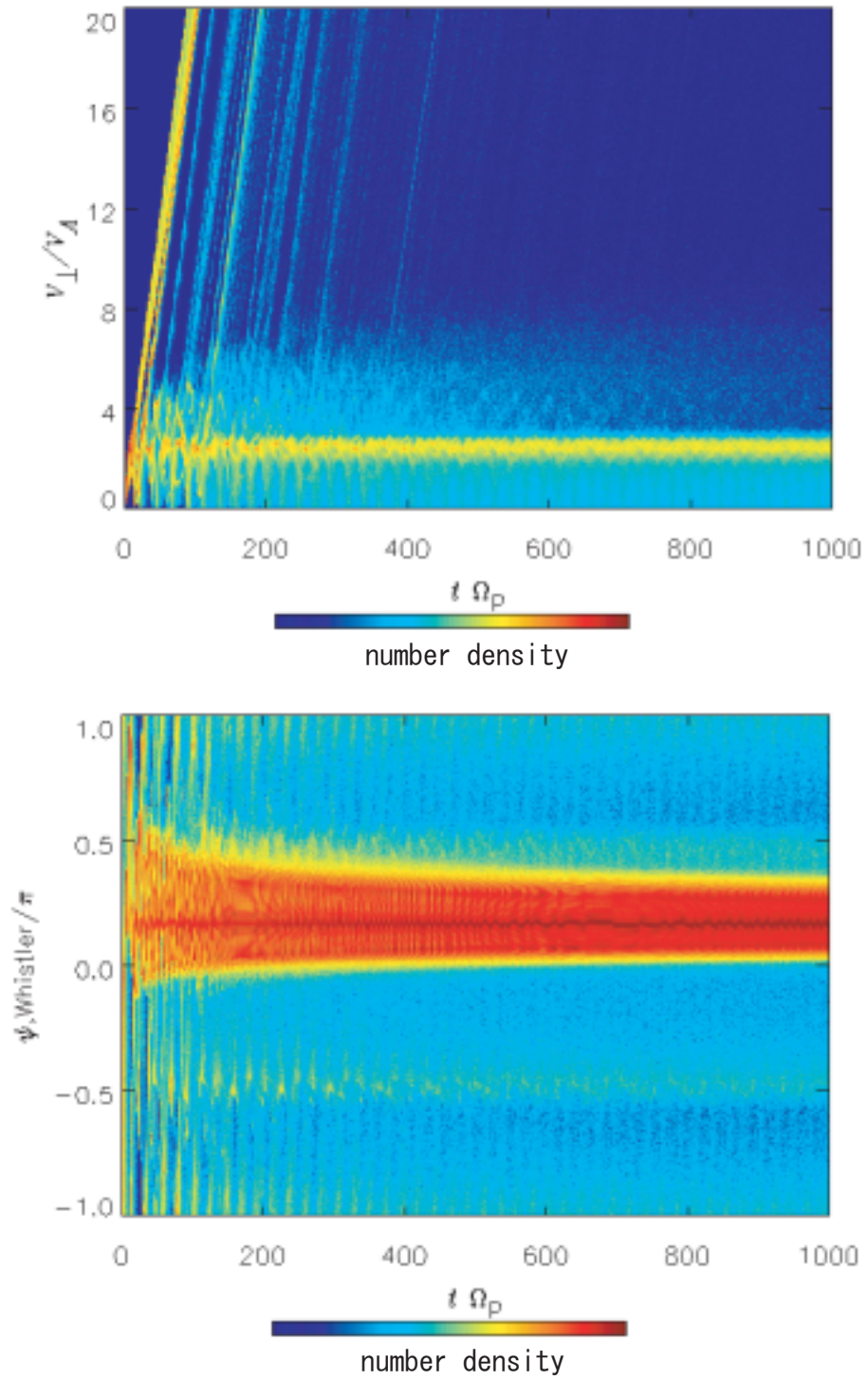


FIG. 13. The time evolution of v_{\perp} (a) and ψ_{Whistler} (b) in the case of the 2 component plasma (black square in Figure 12).